Structural and Magnetic Properties of Cr doped Ni-Zn Nanoferrites Prepared by co-precipitation Method

Ebtesam E. Ateia, L. M. Salah and A. H. El-Bassuony

Physics Department, Faculty of Science, Cairo University, Giza, Egypt

Physical properties of nanocrystalline $Ni_{1-x}Zn_xCr_yFe_{2-y}O_4$, (x=0.3, 0.5 and y=0.0, 0.1) with estimated crystallite size of 16 nm have been studied. XRD pattern of all prepared systems shows that, the nanosamples without Cr^{3+} have a cubic spinel structure with the appearance of small peaks designated as a secondary phase. Magnetic constants such as saturation magnetization, (M_S) remanence magnetization (Mr) and coercive field (Hc) were obtained and reported. The obtained data shows that, the addition of Cr^{3+} (0.1mol) decreases the saturation magnetization. This is due to the decrease of magnetic moment of Cr^{3+} ion (3.0 μ_B) with respect to Fe^{3+} ion (5.85 μ_B). The electrical properties of the investigated samples were also investigated.

1 Introduction

Spinel ferrites have been studied extensively because they play a vital role in the technological applications. Ferrites have good electric properties and a large number of applications from microwave to radio frequency [1]. The dielectric properties of these ferrites are very sensitive to the method of preparation and sintering condition. Therefore, the selection of an appropriate process is the key to obtain high quality ferrites [2].

The interesting magnetic properties of ferromagnetic spinels of the general formula AB_2O_4 are originated mainly from the magnetic interactions between cations in the tetrahedral (A) and the octahedral (B) sites [3].

$ZnFe_2O_4$ is a normal spinel with all the Fe^{3+}ions in the B sites and all the Zn^{2+}ions in the A sites. Whereas $NiFe_2O_4$ has an inverse spinel structure with the Ni^{2+}ions mainly in the B sites and Fe^{3+}ions distributed almost equally between the A and the B sites [4]. Ni Zn has a mixed spinel type of structure. However, in many nano-sized ferrites, the dependence of the particle size on cation distribution is also observed [5],[6]. The spinel structure allows us to introduce different metallic ions, which can change the magnetic and electric properties [7]. Generally, the anti-ferromagnetic nature of Cr^{2+}ions, leads to the possibility of

controlling the magnetic parameters like remanence and coercivity in developing technologically important materials [8]. The investigated samples $Ni_{1-x}Zn_xCr_yFe_{2-y}O_4$, (x=0.3, 0.5 and y=0.0, 0.1) are prepared by co-precipitation method. Improving the structural, magnetic and electrical properties of the investigated samples is the main target of the present work.

2. Materials and Methods

The elements which were used in this work and some of their properties were reported in Table I [9],[10].

Table (1): Some Properties of the elements which were used in the ferrite sample of the present work.

Element	Electronic configuration	Ionic Radius (Å)	Ionization Potential (kcal mol^{-1})	Melting point (^oC)	Boiling point (^oC)	Magnetic Type
$^{58.693}Ni_{28}$	$[Ar]3d^8 4s^2$	0.690	176	1455.00	2913	Ferromagnetic
$^{65.39}Zn_{30}$	$[Ar]3d^{10} 4s^2$	0.600	216	419.53	907	Diamagnetic
$^{51.996}Cr_{24}$	$[Ar]\ 3d^5 4s^1$	0.615	156	1907.00	2671	Antiferromagnetic
$^{55.847}Fe_{26}$	$[Ar]\ 3d^6 4s^2$	(0.645)o (0.490)t	182	1538.00	2861	Ferromagnetic

Synthesis

The samples under investigation samples $Ni_{1-x}Zn_xCr_yFe_{2-y}O_4$, (x=0.3, 0.5 and y=0.0, 0.1) were prepared by co-precipitation method. All ingredients were taken in stoichiometric proportion. The initial ingredients were nickel chloride, zinc chloride, chromium (III) chloride and iron (III) chloride. The co-precipitating agent, sodium hydroxide aqueous solution, in required quantity was added drop by drop to the precursor under continuous stirring till a massy precipitate was formed. The pH was adjusted to ensure completion of the precipitation. The precipitate was washed with deionized water to remove the base and final washing was done with acetone to eliminate water. The filtrate was dried at room temperature to obtain nano ferrite powder. All the powders prepared were calcined at 600^{o}C for 2 hrs with heating rate of 4^{o}C/min.

Sample's characterization

All the prepared samples were identified by x- rays diffractometer (XRD) using Co-Kα radiation (λ=1.79026 Å). The nanoparticles average sizes were estimated using Scherrer's relationship[11].

Infrared spectrophotometer using (perkin- Elmer 1430) in the range from 200 to 1000cm^{-1} with a resolution of 1–5cm^{-1} was used. Morphology and the particle's size of the prepared nanoparticles were investigated using scanning electron microscopy (Philips, XL30 FEG SEM) with magnification up to 150000X and resolution 1.2nm. Magnetic hysteresis measurements were performed by maximum field 5 kOe using Vibrating Sample Magnetometer (VSM) . The ac conductivity for the investigated samples was carried out using LCR Hi Tester (HIOKI model 3531Z Japan). The accuracy of measurement was better than 1%.

3. Results and Discussion

A. Structural Analyses:

X-ray Analysis:

Figure (1) shows the XRD pattern for the $Ni_{1-x}Zn_xCr_yFe_{2-y}O_4$, (x=0.3, 0.5 and y=0.0, 0.1) nano ferrite.

As shown from the Fig.(1), the nanosamples without Cr^{3+} have a cubic spinel structure with the appearance of small peaks designated as a secondary phase. However, in the case of samples containing 0.1 mol of Cr^{3+}, a complete formation of the spinel phase appears without any secondary phases**.** This means that, the addition of 0.1 Cr^{3+} eliminates all the secondary phases of the investigated samples. Also, it is clear from the figure that, the addition of Cr^{3+} leads to increase the enlargement of peaks consequently to the decrease in crystallite size. Whereas, for low Zn^{2+} ion concentration (x=0.3), the broadening of the peaks shows a reasonable increase which reflects better homogeneity and smaller particle size.

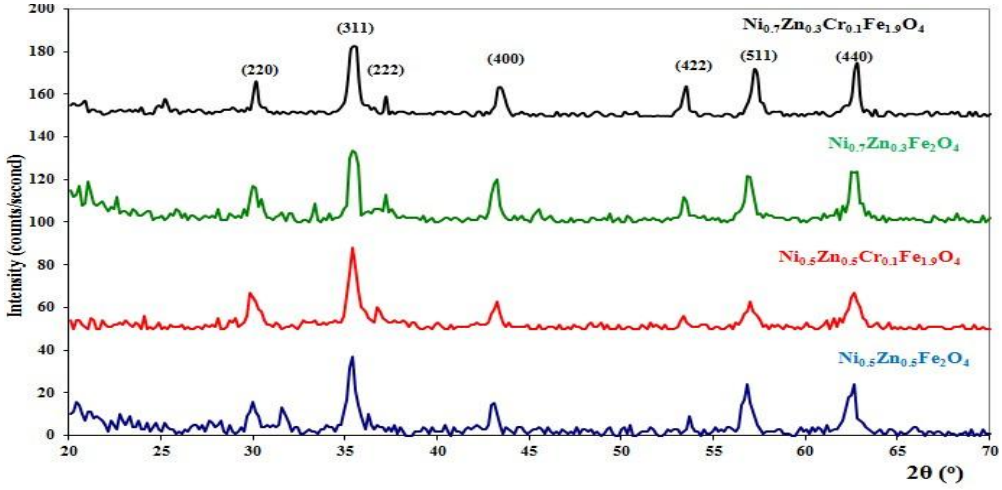

Fig.(1): X-ray powder diffraction pattern for $Ni_{1-x}Zn_xCr_yFe_{2-y}O_4$ nanoferrite, (x=0.3, 0.5 and y=0.0, 0.1)

The molecular weight, the calculated lattice parameter (a), crystallite size, the experimental D_b and the theoretical D_x density, and porosity (P) for $Ni_{1-x}Zn_xCr_yFe_{2-y}O_4$ (x=0.3, 0.5 and y=0.0, 0.1) nanoferrite, are tabulated in Table (2) (the X-ray density was calculated using the relation from reference [12]).

Table (2): Molecular weight, Crystallite size, Lattice parameter (a), X-ray density (Dx), Experimental density (D_b), and Porosity (P) for $Ni_{1-x}Zn_xCr_yFe_{2-y}O_4$ nanoferrite, (x=0.3, 0.5) and (y=0, 0.1).

Composition	Mwt	Crystallite size (nm)	lattice parameter a_{exp} (Å)	X-Ray Density D_x (gm/cm^3)	Experimental Density D_b (gm/cm^3)	Porosity P%
$Ni_{0.5}Zn_{0.5}Fe_2O_4$	237.74	28.0	8.3896	5.339	4.271	20 %
$Ni_{0.5}Zn_{0.5}Cr_{0.1}Fe_{1.9}O_4$	237.35	16.4	8.3891	5.340	4.325	19 %
$Ni_{0.7}Zn_{0.3}Fe_2O_4$	236.40	27.3	8.3867	5.323	4.578	14 %
$Ni_{0.7}Zn_{0.3}Cr_{0.1}Fe_{1.9}O_4$	236.01	15.3	8.3688	5.348	4.706	12%

The data indicate that, the inclusion of Cr^{3+} ion leads to a slight reduction in the lattice parameter. This can be attributed to the effective ionic radii of Cr^{3+} (0.615 Å) whose octahedral coordination is smaller than that of Fe^{3+} (0.645 Å)[9]. From the table it is also clear that, the lattice parameter increases with increasing Zn^{2+} content. This is attributed to the replacement of Fe^{3+} (0.490 Å) on the tetrahedral site by Zn^{2+} (0.600 Å) ions leading to the increase of (r_A). Also, the replacement of Fe^{3+} (0.645 Å) instead of Ni^{2+} (0.690 Å) on the octahedral site helps in decreasing (r_B) [13]. Similar behavior was reported for Ni-Zn ferrite system prepared by Ceramic method[14]. From the table, it could also be said that, $Ni_{0.7}Zn_{0.3}Cr_{0.1}Fe_{1.9}O_4$ have the lowest grain size, highest density and lowest porosity. So the concentration of x=0.3 is the best Zn ions concentration.

IR Analysis:

Infrared spectra for $Ni_{1-x}Zn_xCr_yFe_{2-y}O_4$, (x=0.3, 0.5 and y=0.0, 0.1) are recorded in range 200-1000 cm^{-1} as shown in Fig. (2a,b) and the corresponding data are given in Table 3. The spectra indicate the presence of two absorption bands (ν_1) and (ν_2) as common features of all ferrites[15]. As shown from the Fig.(2) the splitting (multi-bands) of ν_2-band can be attributed to the presence of secondary phase as revealed from XRD pattern. The secondary phases for the investigated samples with x=0.5, y=0.0, appear as multi-bands while the samples with x=0.3, y=0.0, have very small amount of secondary phase which does not appear in IR spectra but it confirmed from XRD analysis as mentioned before. The most important observation is that, the addition of 0.1 mole Cr^{3+} into $Ni_{0.5}Zn_{0.5}Fe_2O_4$ ferrite removes the secondary phase. From the table it is clear that the vibrational bands of the iron ions on both tetra and octahedral positions (ν_1) and (ν_2) are slightly changed depending on Cr^{3+} and Zn^{2+} ion concentration.

Table (3): IR bands Ni1-xZnxCryFe2-yO4 nanoferrite, (x=0.3, 0.5) and (y=0.0, 0.1).

Composition	$\upsilon_1(cm^{-1})$	$\upsilon_2(cm^{-1})$
$Ni_{0.5}Zn_{0.5}Fe_2O_4$	583	347- 400- 470
$Ni_{0.5}Zn_{0.5}Cr_{0.1}Fe_{1.9}O_4$	584	408
$Ni_{0.7}Zn_{0.3}Fe_2O_4$	581	387
$Ni_{0.7}Zn_{0.3}Cr_{0.1}Fe_{1.9}O_4$	582	388

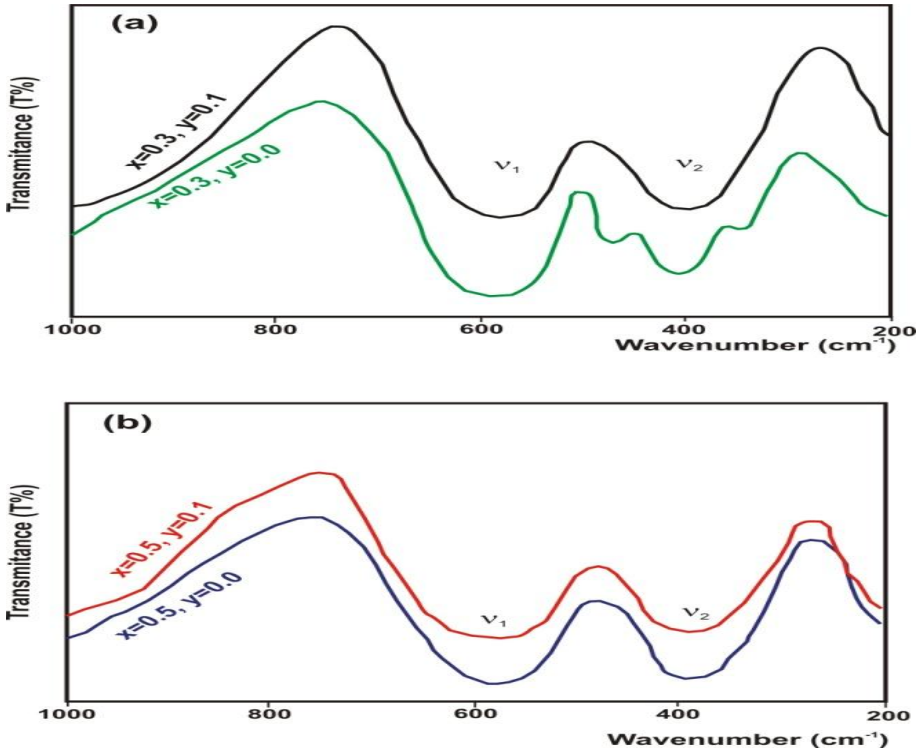

Fig.2(a-b): IR spectra for $Ni_{1-x}Zn_xCr_yFe_{2-y}O_4$ nanoferrite, (x=0.3, 0.5 and y=0.0, 0.1)

Scanning Electron Microscope (SEM) Analysis:

Figure (3 a-d) shows the SEM images for $Ni_{1-x}Zn_xCr_yFe_{2-y}O_4$, (x=0.3, 0.5 and y=0.0, 0.1) nano ferrite. From the Figure, we notice that, the nanocrystalline samples have uniformly distributed spherical shape, some of them are agglomerated. Some shaded areas exist due to voids. The addition of Cr^{3+} increases the homogeneity of the investigated system as shown from the Fig.(3). In fact it is very difficult to use SEM quantitatively to estimate the ultrafine grain size due to agglomeration. SEM micrographs give qualitative information about the crystallite size, shape, pores volume and distribution.

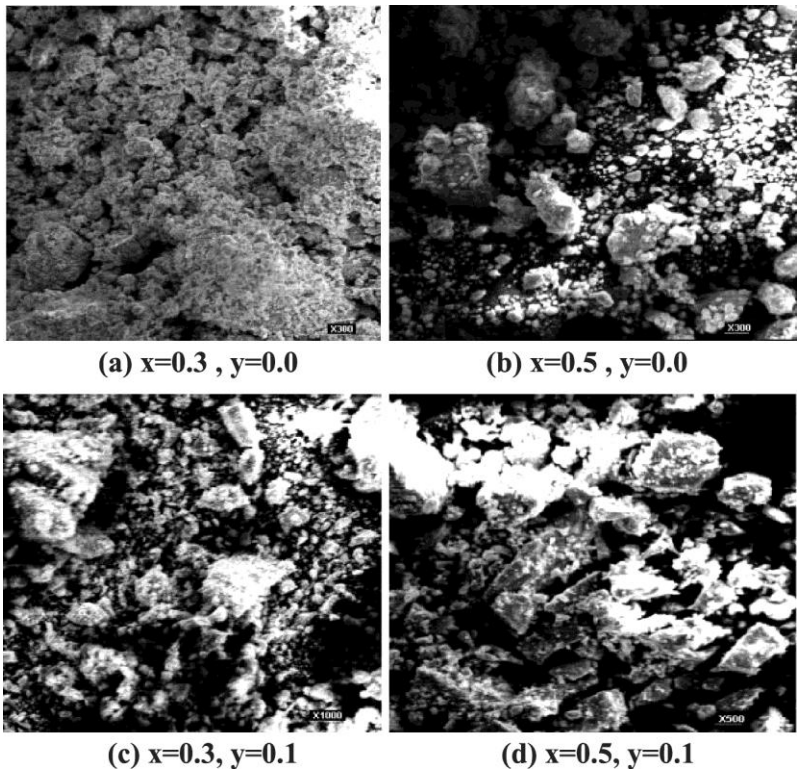

Fig. (3a-d): SEM micrographs for $Ni_{1-x}Zn_xCr_yFe_{2-y}O_4$ nanoferrite, (x=0.3, 0.5 and y=0.0, 0.1).

These characteristics confirm the narrow grain size distribution in the ferrite which is an industrial requirement. Generally, Fe^{2+} ions accelerate the growth rate of the grains [16,17]. Its action may be compensated by the presence of Zn^{2+} ions which act as growth inhibitor. As zinc content increases, the agglomerates decrease and the particles have definite grain boundaries (as shown in Fig.3b), which reveals that Zn serves as an effective sintering aid.

B. Magnetic Properties:

The room temperature magnetization for $Ni_{1-x}Zn_xCr_yFe_{2-y}O_4$ (x=0.3, 0.5 and y=0.0, 0.1) prepared by co-precipitation method is represented in Fig.4(a-d). The figure indicates that Ni-Zn-Cr is a soft magnetic material with minimal hysteresis. The coercive field (H_c), saturation magnetization (M_s), remanence magnetization (M_r), and The squareness ratio (M_r/M_s) for the investigated samples are calculated and tabulated in Table (4). The obtained data show that, the addition of Cr^{3+} (0.1mol) decreases the saturation magnetization. This decrease is due to the smaller magnetic moment of Cr^{3+} ion (3.0 μ_B) as compared to that of Fe^{3+} ion (5.85 μ_B) [18].

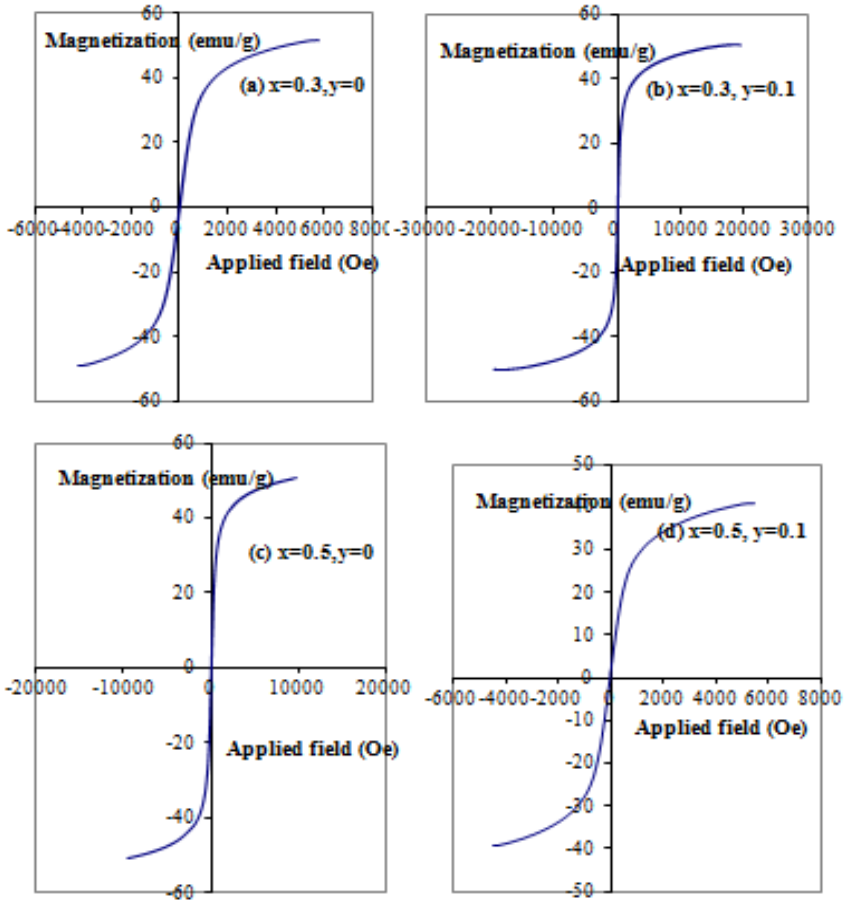

Fig. (4 a-d): Room temperature magnetic hysteresis loops for $Ni_{1-x}Zn_xCr_yFe_{2-y}O_4$ nanoferrite, (x=0.3, 0.5 and y=0, 0.1) .

TABLE (4): coercive field (Hc), saturation magnetization (Ms), remanence magnetization (Mr) and the squareness (Mr/Ms) for $Ni_{1-x}Zn_xCr_yFe_{2-y}O_4$ nanoferrite, (x=0.3, 0.5 and y=0.0, 0.1).

Composition	H_c (Oe)	M_s (emu/g)	M_r (emu/g)	M_r/M_s
$Ni_{0.5}Zn_{0.5}Fe_2O_4$	29.5	50.5	2.51	0.049
$Ni_{0.5}Zn_{0.5}Cr_{0.1}Fe_{1.9}O_4$	16.5	40.7	4.60	0.113
$Ni_{0.7}Zn_{0.3}Fe_2O_4$	19.40	51.5	8.31	0.162
$Ni_{0.7}Zn_{0.3}Cr_{0.1}Fe_{1.9}O_4$	28.5	50.6	2.41	0.048

The same trend is obtained with increasing Zn^{2+} ion concentration (x=0.5). The increase of diamagnetic Zn^{2+} ions in A- sites lead to migration of Fe^{3+} ions from the A-sites towards B-sites. The weakening of A-B exchange coupling that result from this migration, besides increasing the interaction distances leads to a decrease in the magnetic moment. On the other hand, the decrease of the

saturation magnetization of the investigated nanosamples can also be explained on the basis of canted spin or spin glass like layer due to the larger fraction of surface to volume atoms in the smaller particles at the surface of nanoparticles [19].

C .Electrical Properties:

The variation of ln σ with the reciprocal of the absolute temperature (1000/T) for the investigated nanosamples $Ni_{1-x}Zn_xCr_yFe_{2-y}O_4$, (x=0.3, x=0.5 and y=0.0, 0.1) at different frequencies is represented in Fig. 5(a-d). It can be seen that, the ac conductivity increases with increasing temperature ensuring the semiconducting nature of the nanosamples, also it increases with increasing frequency. In other words the frequency is acting as a pumping force to the charge carriers between different localized states and these charge carriers participate in the conduction process.

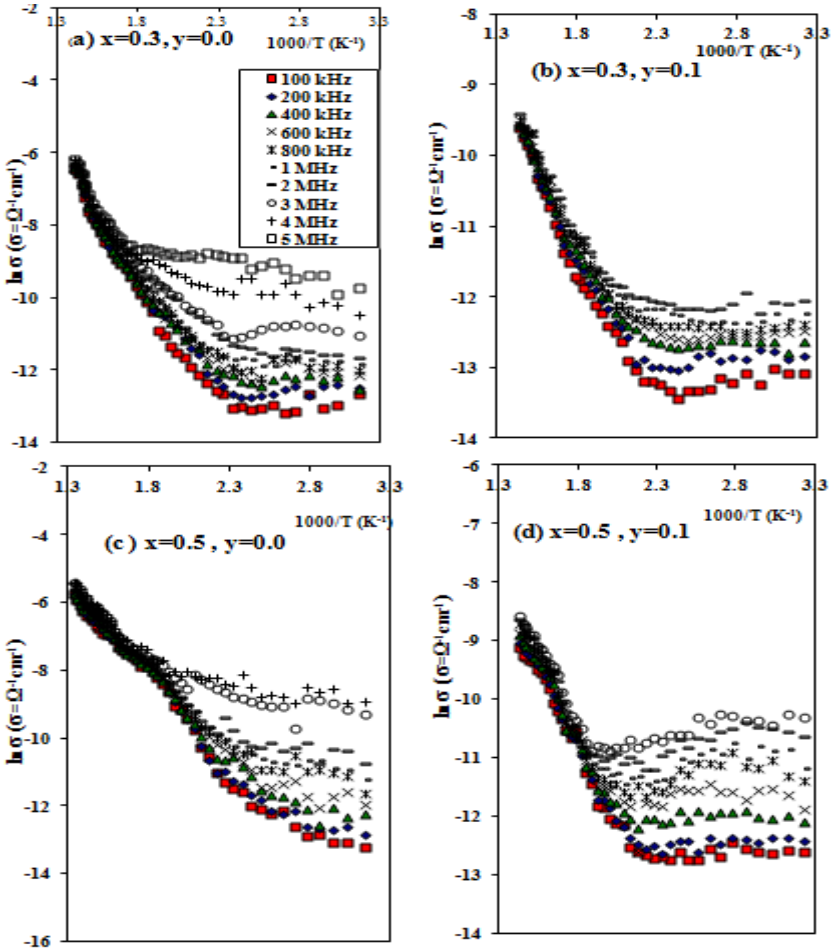

Fig.5: (a-d): Temperature dependence of AC conductivity as function of frequency for $Ni_{1-x}Zn_xCr_yFe_{2-y}O_4$ nanoferrite, (x=0.3, 0.5 and y=0.0, 0.1).

Generally, the electron hopping between B- and A-sites have very small probability compared to that of B-B hopping. The highest value of (σ) is obtained for the nanosample with (x=0.3, y=0.0). This result is explained on the basis of the conduction mechanism that is explained in terms of the electron hopping between $Fe^{3+} \leftrightarrow Fe^{2+}$ ions, (for n-type) and hopping between $Ni^{3+} \leftrightarrow Ni^{2+}$ (p-type) on B-sites. Since chromium ions have preference for octahedral site, thus lead to reduction in electron hopping and therefore decreasing (σ).

Finally, low values of conductivity around room temperature indicate that the studied compositions may be good candidates for the microwave applications that require negligible eddy currents [20].

The values of activation energy and grain sizes are listed in Table (5), where E_f is the activation energy corresponding to the ferrimagnetic region and E_p is corresponding to the paramagnetic region. From the table, it appears that, the activation energies in paramagnetic region are larger than that of ferromagnetic one. This means that, in the paramagnetic region a large energy is needed to liberate the trapped charges and activate them to participate in the conduction process[21]. This can be attributed to the disordered states of the paramagnetic region and the ordered states of the ferrimagnetic region.

Table (5): ACTIVATION ENERGY AT CONSTANT FREQUENCY IN THE LOW (EF) AND HIGH (EP) TEMPERATURE REGIONS RESPECTIVELY FOR NI1-XZNXCRYFE2-YO4 (X=0.3, 0.5 AND Y=0.0, 0.1).

Composition	E_f (eV)	E_P (eV)	Crystallite size (nm)
$Ni_{0.5}Zn_{0.5}Fe_2O_4$	0.23	0.29	28.0
$Ni_{0.5}Zn_{0.5}Cr_{0.1}Fe_{1.9}O_4$	0.29	0.36	16.4
$Ni_{0.7}Zn_{0.3}\ Fe_2O_4$	0.21	0.26	27.3
$Ni_{0.7}Zn_{0.3}Cr_{0.1}Fe_{1.9}O_4$	0.24	0.32	15.3

This result also suggests that the conduction process is affected by the change in magnetic ordering.

As shown from the table, the activation energy of the investigated nanoferrite samples increases with increasing Zn^{2+}, Cr^{3+} content and also with increasing particle size.

D. Dielectric Properties:

Figure (6 a-d) illustrates the variation of the dielectric constant (έ) with the absolute temperature as a function of frequency ranging from 100 kHz to 5 MHz for $Ni_{1-x}Zn_xCr_yFe_{2-y}O_4$, (x=0.3, 0.5 and y=0.0, 0.1). The general trend of all investigated nanoferrite samples is the increase in (έ) with increasing temperature up to transition temperature[22] then decreases. The decreases in the values of (έ) take place depending on addition of Zn^{2+} or Cr^{3+} content. In the lower temperature region up to ≅ 650 K, for all investigated samples, (έ) increases slowly with temperature because the thermal energy given to the sample is not sufficient enough to free the localized dipoles to be oriented in the field direction. Above ≅ 650 K, by increasing temperature, the (έ) increases up to maximum value. This increase is due to large number of dipoles that become free with such high thermal energy and the field aligned them in its direction. The decrease of (έ) is attributed to the decrease in internal viscosity of the system giving rise more degrees of freedom to the dipoles with the result of increasing the disordering in the system and hence decreasing (έ) again. Generally, the electron hopping between B- and A-sites have very smaller probability compared to that for B-B hopping. The highest value of (έ) is obtained for the nanosample with x=0.3, y=0.0. This result is explained on the basis of the conduction mechanism that is explained in terms of the electron hopping between $Fe^{3+} \leftrightarrow Fe^{2+}$ ions, (for n-type) and hopping between $Ni^{3+} \leftrightarrow Ni^{2+}$ (p-type) on B-sites causing local displacements of electrons or holes in the direction of the applied electric field which increase the polarization giving rise the value of (έ). As Zn^{2+} ion substitution increases, (x=0.5) some of Fe^{3+} ions are forced to migrate from A-sites to B-sites[23]. As a result, the number of the electron exchange interaction between Fe^{2+} and Fe^{3+} ions on octahedral sites increases while the number of hole exchange interaction between Ni^{2+} and Ni^{3+} ions decreases. Also chromium ions have a preference for octahedral site, thus they reduce the Fe^{3+} ions in the B-site and in turn reducing Fe^{3+} - Fe^{2+} hopping. Therefore, addition of Cr^{3+} ions to the system decreases Fe^{3+} ions on the octahedral site, decrease polarization, and hence decreasing (έ) as shown from Fig.6(a-d). One can expect that, Ni^{2+} ions play a significant role in polarization and conduction process in low temperature region. While the transition peaks which appeared at high temperature can be attributed to cation-anion-cation interaction over the octahedral position which occurs between 3d orbital of the transition element and 2p of oxygen as a result of application of an alternating electric field[24]. These interaction can be designated as (Ni^{3+}—O^{2-}—Ni^{2+}) and(Fe^{3+}—O^{2-}—Fe^{2+}).

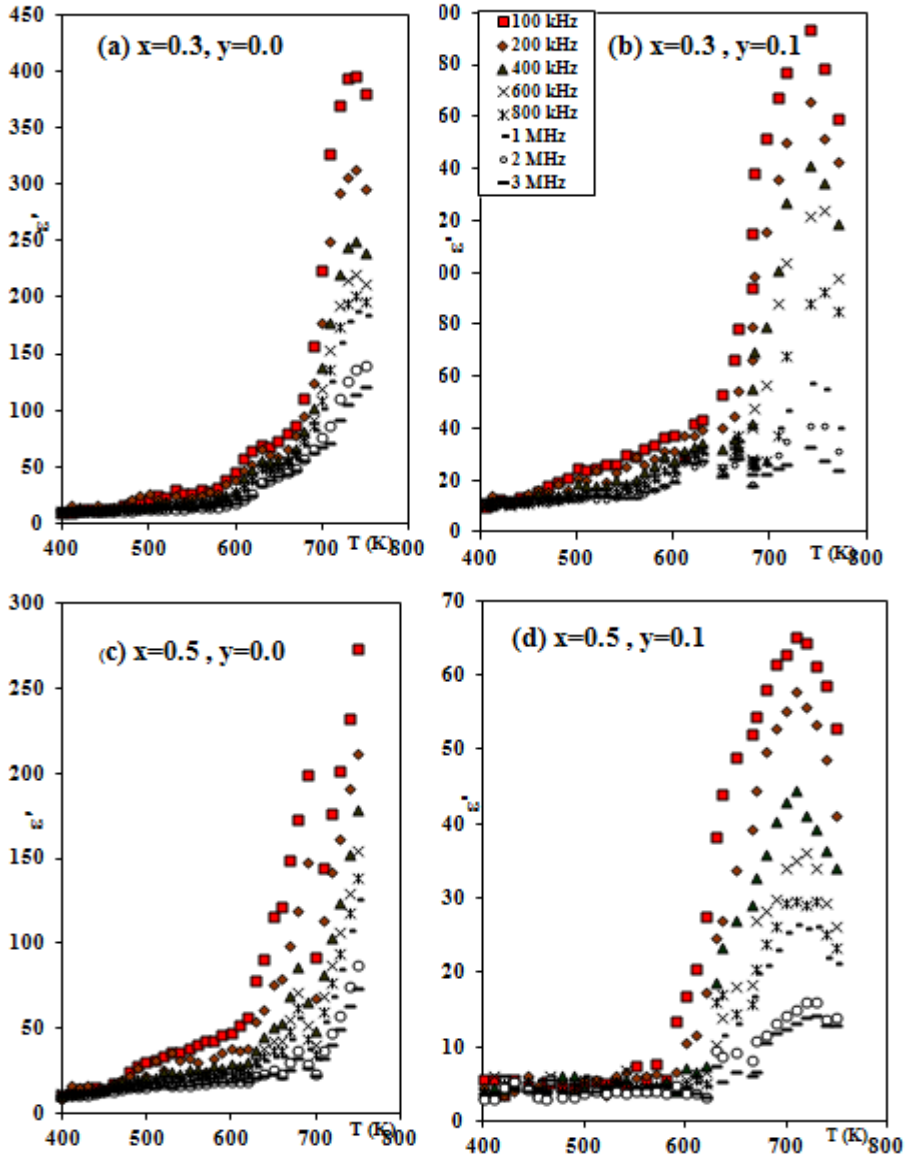

Fig. 6 (a-d): Temperature dependence of real part of dielectric constant (ε') for $Ni_{1-x}Zn_xCr_yFe_{2-y}O_4$ nanoferrite, (x=0.3, 0.5 and y=0.0, 0.1).

The variation of the dielectric constant (έ) with frequency for the investigated nanosamples at different temperature are shown in Fig.(7 a-d). It is clear that, dielectric constant (έ) decreases with increasing frequency while increases with increasing temperature which is in good agreement with several investigations[25]. The nanosamples reveal dispersion due to Maxwell-Wagner interfacial polarization[26-27] which are in good agreement with Koop's

phenomenological theory[28]. The data shows that, the dispersion of the dielectric constant with frequency is maximum for the sample with (x=0.3 and y=0.0). A comparison of the dispersion curves show that the change in the values of the dielectric at lower frequencies of the applied field are larger than that at higher frequencies. The observed variation in the dielectric relaxation intensity can be explained on the basis of space charge polarization due to the inhomogeneous dielectric structure of the samples as discussed by Maxwell[26] and Wagner[27], as the frequency of the externally applied field increases. Gradually, though the number of ferrous ions is present in the nanoferrite material, the dielectric constant decreases. This reduction occurs because beyond a certain frequency of the externally applied field the electronic exchange between ferrous and ferric ions cannot follow the alternating field [29].

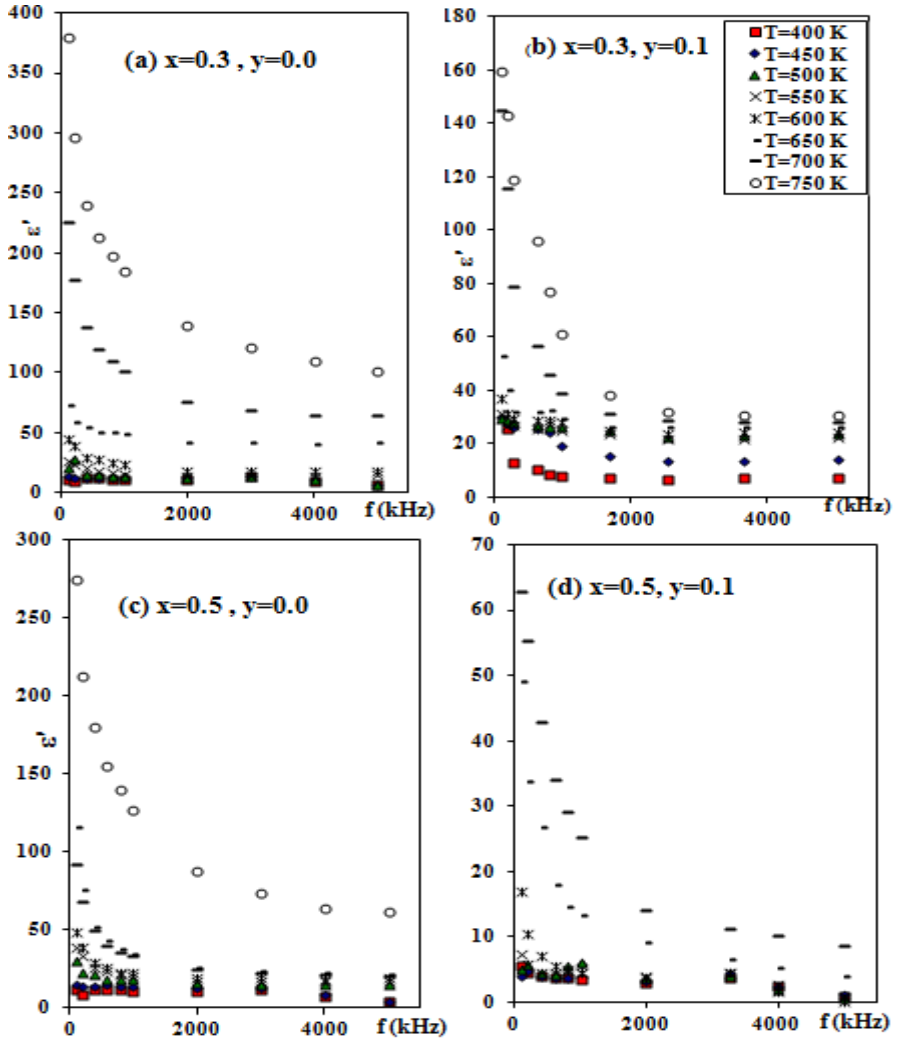

Fig. 7: (a-d): Frequency dependence of real part of dielectric constant (ε') with frequency for the investigated nanosamples at different temperature

Figure (8 a-d) shows the dielectric loss factor (ε″) with the absolute temperature as a function of the applied frequency for the nanosamples $Ni_{1-x}Zn_xCr_yFe_{2-y}O_4$, (x=0.3, 0.5 and y=0.0, 0.1). The figure shows a continuous increase in (ε″) with temperature until reaching maximum then decreases. The increase in (ε″) with temperature is due to the relaxation of the dipole molecules in cooperation with the resulting drop in the relaxation time. This in turn exerts a double effect on the dielectric loss factor, on one hand the friction between the dipoles will be increased and on the other hand, the energy required to overcome the internal mechanical friction of the medium will be decreased when the dipole rotates through a unit angle. The maximum in the dielectric loss occur at relatively low frequencies and decreases with increasing frequency. The broad peak disappears at higher frequencies. A broad peak of the dielectric loss indicates the existence of a distribution of relaxation time rather than a single relaxation time[30]. Experimental results with the loss factor having high values at appropriate temperatures give the samples importance in terms of technologic low frequency applications. Likewise, a potential in terms of high frequency applications may also be mentioned due to the low dielectric losses. The occurrence of loss peaks can be discussed in view of the strong correlation between the conduction mechanism and the dielectric behavior for the spinel ferrite as Iwauchi[31] pointed out. The conduction mechanism in the investigated nanosamples is explained in terms of the hopping conduction process which occurs among the octahedral B-sites. In this case a maximum in (ε″) is observed when the hopping frequency is equal to the external electric field frequency[32]. The figure shows also a continuous increase in the dielectric loss with increasing Zn content (x=0.5). This may be due to cluster formation which acts as trapping centers of different depths. This is confirmed from SEM analysis.

The variation of dielectric loss (ε″) with frequency is shown in Fig. (9 a-d). The loss decreases continuously with increasing frequency and attains a constant value at higher frequencies. At higher frequencies, losses are found to be low domain wall motion which is inhibited and magnetization is forced to change by rotation. The dispersion in (ε″) is seen in lower frequency region. A maximum value in (ε″) can be observed only when the hopping frequency is equal to that of the externally applied electric field. The dielectric loss decreases inversely as the frequency increases. It can further observed that, the dielectric loss decreases with decreasing Zn^{2+} content, i.e the value of (ε″) for $Ni_{0.5}Zn_{0.5}Cr_{0.1}Fe_{1.9}O_4$ is larger compared to that of $Ni_{0.7}Zn_{0.3}Cr_{0.1}Fe_{1.9}O_4$ at the corresponding temperature.

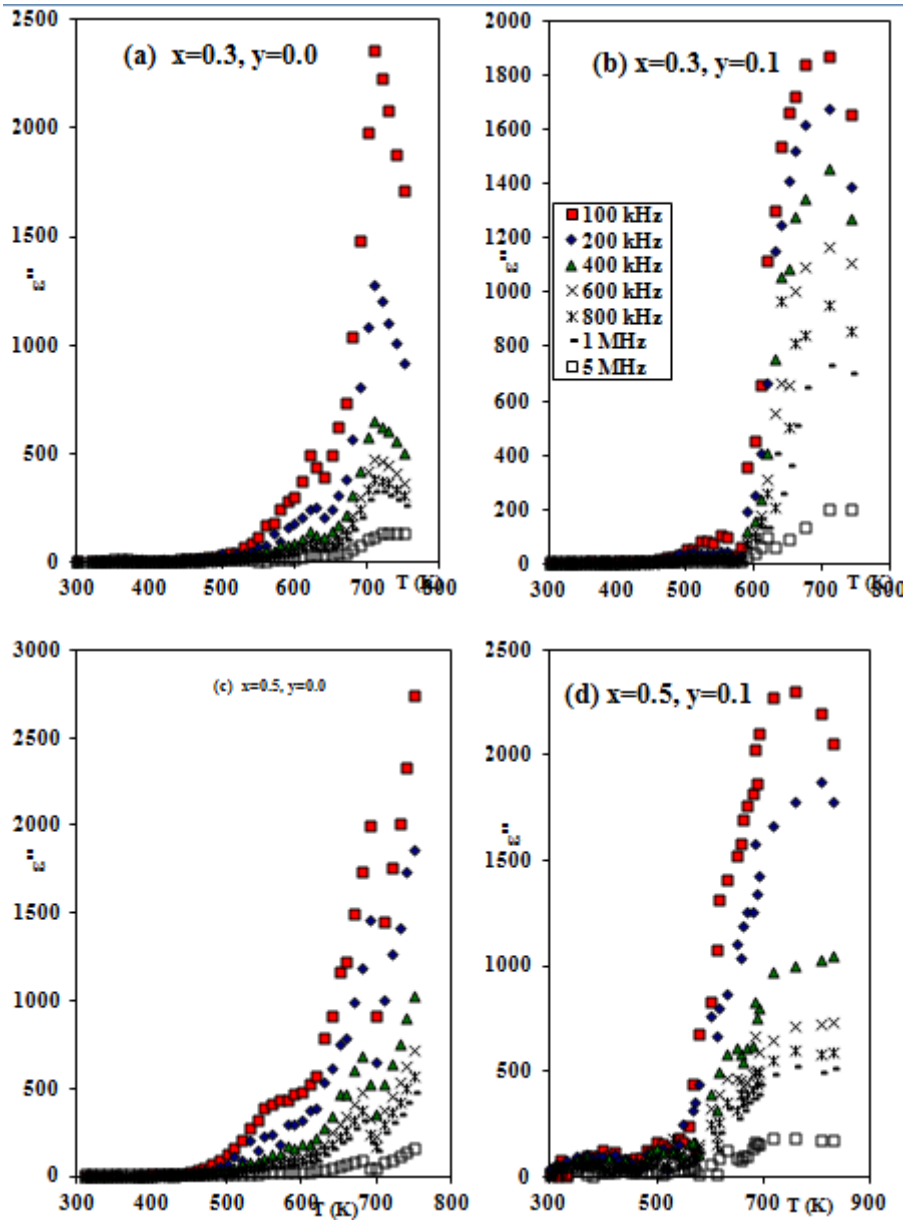

Fig. (8): (a-d): Temperature dependence of dielectric loss factor (ε″) for $Ni_{1-x}Zn_xCr_yFe_{2-y}O_4$ nanoferrite, (x=0.3, 0.5 and y=0.0, 0.1).

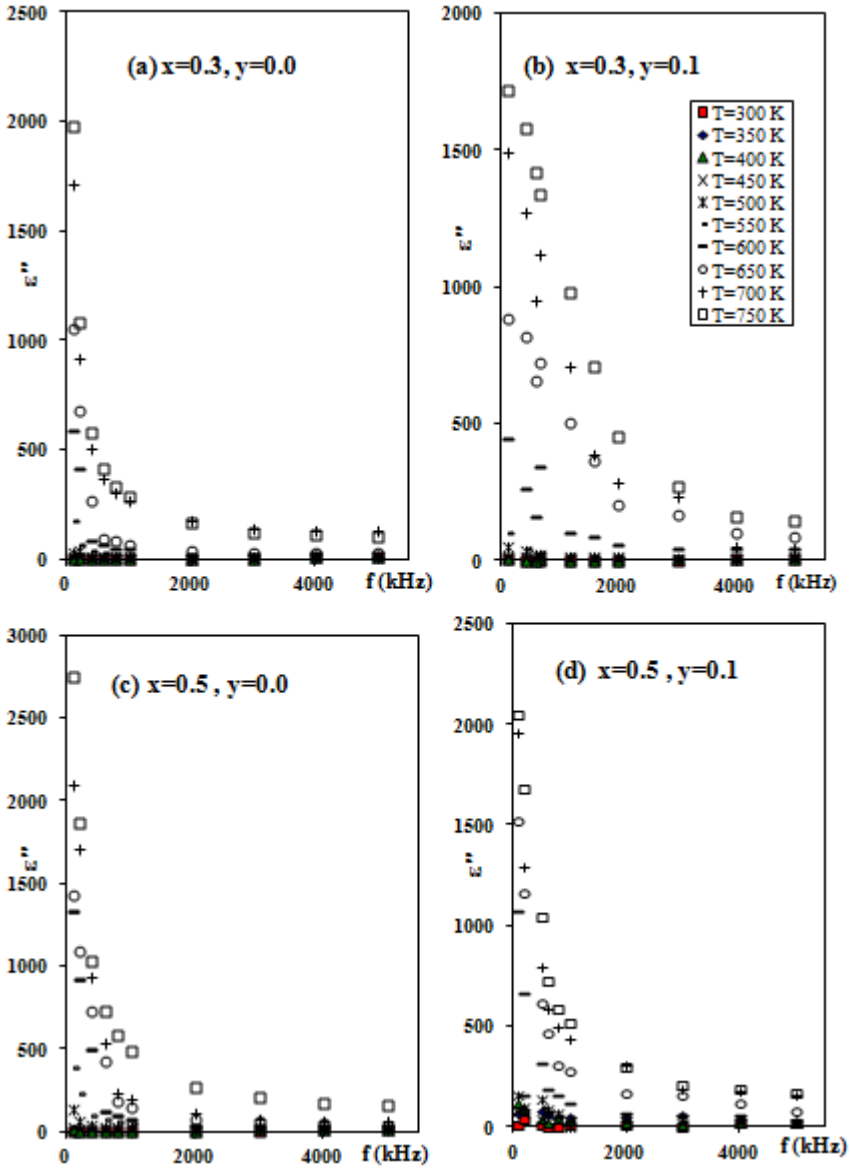

Fig. (9): (a-d): Frequency dependence of dielectric loss factor (ε″) with frequency for the investigated nanosamples at different temperature.

4. Conclusion

1. The addition of 0.1 Cr^{3+} eliminates all the secondary phases of the investigated samples.
2. The replacement of iron with chromium ion at octahedral sites in the ferrite leads to decrease in cation vacancies, porosity and grain size while it increases the bulk density.

3. The real part of dielectric constant (ε′) for all investigated samples increases with increasing temperature up to a certain value of temperature (transition temperature) and decreases with frequency.
4. The Cr^{3+} ions do not participate in the conduction mechanism but limit the degree of $Fe^{2+} \leftrightarrow Fe^{3+}$ transfer, thereby obstructing electron hopping.
5. The increase in electrical resistivity, saturation magnetization , remanence and the decrease in coercivity suggests that, the samples synthesized by the co-precipitation method are suitable for microwave devices and high density recording media applications .

References

1. J. Chand, G. Kumar, P. Kumar, S. K. Sharma, M. Knobel, and M. Singh, *J. Alloys and Compds.*, **509**, 9638 (2011).
2. G. Kumar, J. Chand, S. Verma, and M. Singh *J. Phys. D: Appl. Phys.*, **42**, 155001 (2009).
3. C. Subhash, B.K. Srivastava, and K. Anjali *Indian J. Pure & Appl. Phys.*, **42**, 366 (2004).
4. F. Van der Woude, and G. A. Swatzky *Phys. Rev. B***, 4**, 3159 (1971).
5. G.A. Petitt, and D.W. Forester, *Phys. Rev. B,* **4**, 3912 (1971).
6. S.M. Yusuf, V.C. Sahni, and L.M. Rao, *J. Phys.: Condens. Matter*,**7**, No. 5, 873 (1995).
7. C.N. Chinnasamy, A. Narayanasamy, N. Ponpandian, K. Chattopadhyay, K. Shinoda, B. Jayadevan, K. Tohji, K. Nakatsuka, T.Furubayashi, and I. Naktani, *Phys. Rev. B*, **63**, 184108 (2001).
8. T.T. Ahmed, I.Z. Rahman, and M.A. Rahman, *J. Mater. Process. Technol.*, **153**-154, Nov. 797 (2004).
9. R. D. Shannon, *Acta Crystallogr.*, **A32**, Sept. 751 (1976).
10. Periodic Table, SARGENT-WELCH, Scientific Company, 7300 Linder Avenue, Skokie, Illinois 60076, Catalog Number s-18806.
11. B. D. Cullity, *"Elements of X-ray Diffraction"*, third ed., Prentice-Hall, Inc., New Jersey, p. 388 (2001).
12. L. M. Salah, A.M.Moustafa and I.S. Ahmad Farag, *Ceramics International*, **38,** 5605 (2012).
13. C. M. Strivastava, S. N. Shringi, M. S. Patani, and S. M. Joglekar, *Bull. of Mater. Sci.*, **6,** 7 (1984).
14. Saiduzzaman, M. A. Hossain, A. K. M. Hakim, S. Noor, R. Islam, and M. Al-Mamun, *J. Mater. Sci. and Eng. B,* **1**, No. 7B, 891 (2011).
15. R. D. Waldron, *Phys. Rev.*, **99**, (1955) 1727
16. R. Valenzuela, *"Magnetic Ceramics"*, Cambridge University, 11 (1994).
17. T. Komada, T. Itoh, M. Tabata, and Y. Tamaura, *J. Appli. Phys.*, **69**, No. 8, 5915 (1991).

18. Y. H. Han, J. J. Suh, M. S. Shin and S. K. Han, *J. Phys. IV France*, **7**, C1-111 (1997).
19. S. B. Waje, M. Hashim, W. D. W. Yusoff, and Z. Abbas, *J. Magnet. and Magnet. Mater.*, **322**, 686 (2010).
20. M.A. Elkestawy, *J. Alloys and Compounds*, **492**, 616 (2010).
21. S.M. Patangea, E. S. Sagar, K.S. Lohar, S.S. Jadhav, N. Kulkarni, and K.M. Jadhav, *Physica B*, vol. **406,** 663 (2011).
22. A. V. R. Reddy, G. R. Mohan, B. S. Boyanov and D. Ravinder, Materials Letters, **39,** 153 (1999).
23. J. S. Bijal and D. Kothari, Solid State Communications, **83,** 679 (1992).
24. J. B. Goodenough, *Physical Review*, **6,** 1442 (1960).
25. D. Ravinder and A. C. Reddy, Materials Letters, **57,** 2855 (2003).
26. J. A. Maxwell, *Treatise on Electricity and magnetism, Clarendon Press, Oxford, London*, (1982).
27. K. W. Wagner, Annalen der Physik, (Leipzig), **40,** 817 (1913).
28. C. G. Koop, *Physical Review*, **83,** 121 (1951).
29. G. R. Mohan, D. Ravindr, A.V. R. Reddy and B. S. Boyanov, *Materials Letters*, **40,** 39 (1999).
30. D. El-Kony, *Egypt Journal of Solids*, **27,** 2 (2004).
31. K. Iwanchi, *Journal of Applied Physics***, 10,** 1520 (1971).
32. M. A. Ahmed, S. F. Mansour and M. Afifi, *Journal of Magnetism and Magnetic Materials*, **324,** 4 (2012).